J|A|C|S
COMMUNICATIONS

Published on Web 07/16/2004

Metal Latticeworks Formed by Self-Organization in Oscillatory Electrodeposition

Shuji Nakanishi, Kazuhiro Fukami, Toshio Tada, and Yoshihiro Nakato*

Division of Chemistry, Graduate School of Engineering Science, Osaka University, Toyonaka, Osaka 560-8531, Japan

Received May 20, 2004; E-mail: nakato@chem.es.osaka-u.ac.jp

Self-organized formation of ordered micro- and nanostructures of metals and semiconductors at solid surfaces has been attracting keen attention in view of nanotechnology.[1,2] Recent studies on nonequilibrium, nonlinear chemical dynamics have proved a large possibility of self-organized formation of a variety of ordered structures such as stripes, dot arrays, and target and spiral patterns,[1−7] but the only patterns ever reported are two-dimensional (2-D) and horizontal, apart from dendrites[8] formed in diffusion-limited metal deposition. The formation of organized "vertical" structures and further organized 3-D structures will need novel strategies. Electrochemical systems have an advantage in that they can provide spatially nonlocal and global coupling.[9,10] In this communication, we report that strikingly well-ordered metal latticeworks, standing perpendicular to the substrate, are formed spontaneously in oscillatory electrodeposition through cooperation of various processes with long-range spatiotemporal synchronization. The principle is unique, is never realized by other methods, and opens a new, promising way for nanostructuring.

Figure 1 shows (A) an optical microscopic (OM) image of the latticeworks of deposited tin (Sn), together with (B) a schematic illustration of the deposit structure. Deposition experiments were carried out in 0.2 M Sn(II) + 4.0 M NaOH, with a polycrystalline Sn disk being used as the working electrode. When the electrode potential (E) was scanned from positive to negative, a Sn-depositing cathodic current started to flow at about −1.1 V vs Ag/AgCl (sat. KCl) and reached the (potential-independent) diffusion-limited current at about −1.2 V. A potential oscillation appeared when the current density (j_{ex}), regulated externally with a potentio-galvanostat, exceeded the diffusion-limited current density ($j_{diff} \cong -18$ mA cm^{-2}), where the current density was calculated for the apparent flat-surface area of the electrode. The Sn latticeworks of Figure 1 were obtained under oscillating electrodeposition at constant $j_{ex} = -36$ mA cm^{-2}.

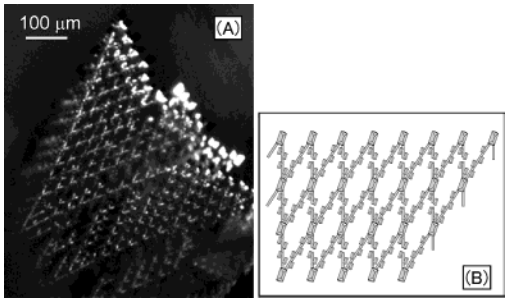

Figure 1. (A) Optical microscopic (OM) image of highly ordered 2-D latticeworks of tin (Sn), produced by oscillation-induced electrodeposition. (B) Schematic illustration of the latticework structure.

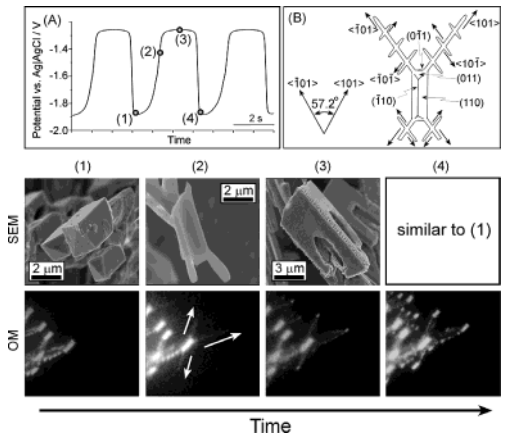

Figure 2. (A) Potential oscillation observed for Sn electrodeposition at a constant externally applied current density $j_{ex} = -36$ mA cm^{-2}. (B) Schematic illustration of crystal faces and directions of tetragonal tin (β-Sn) relevant to the present work. Pictures marked by OM and SEM show optical microscopic (OM) and scanning electron microscopic (SEM) images of Sn deposits, respectively. The numbers (1), (2), (3), and (4) on the pictures indicate that they were taken at a stage of the potential oscillation marked by the same number in (A).

How is such a highly ordered latticework of Sn produced? To answer the question, we inspected growth processes for the Sn latticework during the potential oscillation under in situ conditions with the use of an optical digital microscope (VH-5000, Keyence) and a video camera. In addition, we also inspected pieces of the Sn latticeworks with a high-resolution scanning electron microscope (SEM, Hitachi S-5000) by pulling out the electrode from the electrolyte at various stages of the potential oscillation. Pictures in Figure 2, marked by OM and SEM, show results of such experiments. The numbers (1), (2), (3), and (4) on the pictures indicate that they were taken at a stage of potential oscillation marked by the same number in Figure 2A. Figure 2B schematically shows crystal faces and directions of tetragonal tin (β-Sn), important in later discussion.

On the basis of Figure 2, a correlation between the potential oscillation and the Sn-latticework growth can be explained as follows. At stage (1), just after the electrode potential (E) has shifted toward the negative, the Sn latticework has cuboid crystals at its tips. The cuboid crystals are made of tetragonal tin (β-Sn) and are surrounded with the (110) and (011) faces and equivalents, where the (011) face is the closest-packed, thermodynamically stable face. At stage (2), on the other hand, just after the E has shifted toward the positive, sharp needles grow from three corners of the cuboid crystals in the ⟨101⟩ direction and equivalents. The angle between the ⟨101⟩ and ⟨−101⟩ directions in crystal model for β-Sn is 57.2°, in good agreement with the observed angle between the corresponding two needles in the OM images. The sharp needles have a number of small branches in the ⟨101⟩ direction and equivalents, as schematically shown in Figure 2B. At stage (3), where the E remains on the positive side of the potential oscillation, new cuboid crystals grow at the tips of the sharp needles. Then, when the new cuboid crystals grow enough, the E shifts back toward the negative, and stage (4) is reached. Stage (4) is equivalent to stage (1) except

10.1021/ja047042y CCC: $27.50

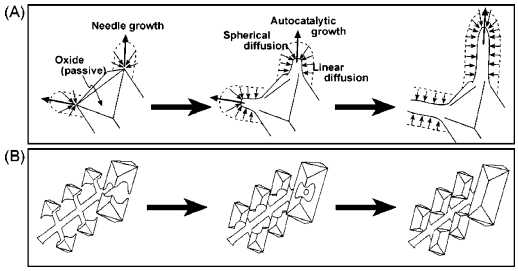

Figure 3. Schematic drawings of Sn crystallites formed in the course of the potential oscillation for explaining the mechanisms of the potential oscillation and latticework formation.

that one layer of the needles and cuboids is added at the tip of the Sn latticework.

Now, we consider mechanisms for the potential oscillation and the Sn-latticework growth. First, we note that the experiment is done under a galvanostatic (constant current-density) condition with $j_{ex} > j_{diff}$. At stage (1), the (110) and (011) faces and equivalents of β-Sn are covered with thin layers of Sn oxide or hydroxide and passivated, as explained later. This implies that the effective area of the active electrode surface (S_{eff}) for Sn deposition becomes small, and thus, the E shifts to the negative until hydrogen evolution occurs (Figure 2A) to maintain the j_{ex}. At such a large negative potential, the potential-regulated rate of electrodeposition of Sn becomes very high; hence, this reaction becomes diffusion limited.

Under the diffusion-limited condition, autocatalytic crystal growth, which is known as a mechanism for Mullins−Sekerka instability,[11] starts (Figure 3A). Namely, under the diffusion-controlled condition, a spherical diffusion layer is formed at a peaked part of the electrode surface. This leads to a high current density at the peaked part, compared with that at the flat parts, and thus to a high growth rate for Sn at the former part. This implies that a peaked part grows rapidly, resulting in formation of sharp needles, as really observed at stage (2). The cuboid crystal of Sn, surrounded with the (110) and (011) faces and equivalents, has four equivalent peaked corners in the ⟨101⟩ direction and equivalents (Figure 2B). One of them is used for a needle supporting the cuboid crystal itself, and therefore, three new needles grow from the remaining three peaked corners at stage (2) (Figure 2). The needle formation occurs mainly at the tips of the Sn latticework, because under the diffusion-controlled condition, almost all Sn(II) ions are exhausted inside the Sn latticework.

The formation of a large number of needles at stage (2), on the other hand, leads to a large increase in the effective area (S_{eff}) of the active electrode surface and, hence, a large decrease in the effective current density (j_{eff}) under the constant externally applied current j_{ex}. The decrease in j_{eff} in turn leads to a positive shift in E, which continues until the autocatalytic crystal growth stops; namely, the diffusion-controlled condition disappears, or the j_{eff} reaches the reaction-limited current density. Accordingly, while the E is on the positive side of the potential oscillation (stage (3)), a normal potential-regulated electrodeposition reaction proceeds under the reaction-limited condition,[12] which leads to production of cuboid crystals surrounded with the thermodynamically stable (110) and (011) faces and equivalents (Figure 3B), together with thickening of the needles. The cuboid-crystal formation also occurs mainly at the tips of the Sn network, similar to the case of needle formation mentioned earlier, because most Sn(II) ions inside the Sn latticework are exhausted at the previous stage of the oscillation. Two cuboid crystals sometimes coalesce with each other, as shown in Figure 3B. Similar coalescence also sometimes occurs between two needles at stage (2), resulting in formation of tetragonal latticeworks (see Figure 1). It should be emphasized that such coalescence arises from a well-ordered periodic latticework structure of Sn crystal, produced by long-range self-organization under the potential oscillation.

At stage (3), there is another important factor that the E is near the redox potential for oxidation of Sn to Sn oxide (−1.2 V vs Ag/AgCl), as is seen from a Pourbaix diagram.[13] Thus, the Sn surface is soon oxidized and passivated. The surface oxidation of Sn may involve an autocatalytic mechanism, because it produces electrically polar bonds, $Sn^{\delta+}-O^{\delta-}$, at the surface and the resultant $Sn^{\delta+}$ atoms induce positive polarization of adjacent surface Sn atoms, which in turn causes an easier attack of negatively charged species OH^- on them. A similar autocatalytic oxidation mechanism was previously reported[14] for H_2O_2 reduction on Pt. Interestingly, the mechanism worked most effectively at the closest-packed surface such as Pt(111). We can thus expect that the Sn-surface oxidation proceeds effectively on the closest-packed (110) and (011) faces or equivalents. This implies that, as soon as the cuboids are covered with these faces, they are instantaneously covered with Sn oxides. The oxidation leads to a decrease in S_{eff} and an increase in j_{eff} under the constant externally applied current, which causes a negative shift in E. Thus, the electrochemical system moves to stage (4).

The above arguments clearly indicate that the formation of well-ordered latticeworks of Sn arises from cooperation of various processes, such as needle formation by autocatalytic crystal growth, cuboid formation under a reaction-limited condition, and autocatalytic oxidation at closest-packed surfaces. The important point is that all the processes are spatiotemporally synchronized under nonequilibrium, nonlinear electrochemical dynamics. This principle is quite unique and is never realized by other methods. The mechanism will generally be applicable to similar oscillatory deposition of metals producing dendrites, such as Zn,[15] Pb, and Cu. We can thus say that the present work has opened a new, promising way toward the formation of highly ordered 3-D micro- or nanostructures at solid surfaces.

Acknowledgment. We thank the Core Research for Evolutional Science and Technology (CREST) program of the Japan Science and Technology Agency (JST) for financial support. This work was partly supported also by a Grant in Aid of the Ministry of Education, Science, Sport, and Culture for scientific research and by the Murata Science Foundation.

References

(1) Notzel, R.; Temmyo, J.; Tamamura, T. *Nature* **1994**, *369*, 131−133.
(2) Kim, S. O.; Solak, H. H.; Stoykovich, M. P.; Ferrier, N. J.; de Pablo, J. J.; Nealey, P. F. *Nature* **2003**, *424*, 411−414.
(3) Frost, F.; Schindler, A.; Bigl, F. *Phys. Rev. Lett.* **2000**, *85*, 4116−4119.
(4) Lev, O.; Sheintuch, M.; Pisemen, L. M.; Yarnitzky, C. *Nature* **1988**, *336*, 458−459.
(5) Li, Y. J.; Oslonovitch, J.; Mazouz, N.; Plenge, F.; Krischer, K.; Ertl, G. *Science* **2001**, *291*, 2395−2398.
(6) Yuzhakov, V. V.; Chang, H. C.; Miller, A. E. *Phys. Rev. B* **1997**, *56*, 12608−12624.
(7) Krastev, I.; Koper, M. T. M. *Physica A* **1995**, *213*, 199−208.
(8) Fleury, V.; Watters, W. A.; Allam, L.; Devers, T. *Nature* **2002**, *416*, 716−719.
(9) Krischer, K.; Mazouz, N.; Grauel, P. *Angew. Chem., Int. Ed.* **2001**, *40*, 851−869.
(10) Christoph, J.; Eiswirth, M. *Chaos* **2002**, *12*, 215−230.
(11) Mullins, W. W.; Sekerka, T. F. *J. Appl. Phys.* **1963**, *34*, 323−329.
(12) The E value on the positive side of potential oscillation in Figure 2A is a little more negative than −1.2 V at which the diffusion-limited current is reached in stationary current−potential curves. This is most probably because of a negative deviation of E by an ohmic drop in the electrolyte during the oscillation with a high current density of -36 mA cm^{-2}.
(13) Pourbaix, M. *Atlas of Electrochemical Equilibria in Aqueous Solutions*; National Association of Corrosion Engineers: Houston, 1974.
(14) Nakanishi, S.; Mukouyama, Y.; Karasumi, K.; Imanishi, A.; Furuya, N.; Nakato, Y. *J. Phys. Chem. B* **2000**, *104*, 4181−4188.
(15) Fukami, K.; Nakanishi, S.; Sakai, S.; Nakato, Y. *Chem. Lett.* **2003**, *32*, 532−533.

JA047042Y